analyzer is mounted on the magnetometer boom of the spinning section of the Galileo spacecraft such that this rotation, together with multiple sensors, provides almost complete coverage of the entire solid angle for charged particle velocity vectors at the spacecraft position. Electronic sectioning divides the rotation into a number of azimuthal sectors that are preselected by ground command. The E/Q range is 0.8 V to 52 kV for positive ions and electrons. The operational mode at Venus is such that 32 E/Q passbands are sampled over this E/Q range during approximately 120° of spacecraft rotation. The spacecraft rotation period is 19.1 s. Typical energy resolution $\Delta E/E$ is 0.11. By control of the spin phase of the above sectors, 32 E/Q samples of intensities within eight azimuthal sectors for each sensor were acquired during four contiguous spacecraft rotations. The spacecraft spin axis was aligned with the direction to the sun to within a few degrees during Venus encounter. A sunshade that is used to prevent overheating of the instrument obscured the fields of view P7 and E7, which were directed most nearly to the solar direction. This sunshade prevents the detection of the solar wind ions and the bulk of the magnetosheath ion distributions.

3. Energy-time (E-t) spectrograms display the counts per accumulation period for each E/Q scan (abscissa) of the instrument. The accumulation period is 0.2 s. For the instrument operation at Venus, 32 samples at equal logarithmic intervals in E/Q were taken. The responses are logarithmically coded according to the two color bars displayed in Fig. 1, one each for the ion and electron analyzers, respectively.
4. T. V. Johnson, *Science* **253**, 1516 (1991).
5. M. G. Kivelson *et al.*, *ibid.*, p. 1518.
6. Values for the solar wind speeds and proton densities from the plasma instrument on Pioneer Venus Orbiter were supplied by J. D. Mihalov of the National Aeronautics and Space Administration Ames Research Center. The electron densities derived from the Galileo plasma instrument have been cross-calibrated with the Langmuir-line frequency observed with the Galileo plasma wave instrumentation (D. A. Gurnett *et al.*, *ibid.*, p. 1522).
7. W. C. Feldman, in *Collisionless Shocks in the Heliosphere: Reviews of Current Research*, B. T. Tsurutani and R. G. Stone, Eds. (Geophysical Monograph 35, American Geophysical Union, Washington, DC, 1985), pp. 195–205.
8. The solar wind electron distribution exhibits a cool core of electrons convecting with the solar wind ions and a suprathermal velocity distribution that includes a magnetic field–aligned "strahl" at higher energies. See, for example, W. G. Pilipp *et al.* [*J. Geophys. Res.* **92**, 1075 (1987)].
9. J. T. Gosling, M. F. Thomson, S. J. Bame, C. T. Russell, *ibid.* **94**, 10011 (1989); R. J. Fitzenreiter, J. D. Scudder, A. J. Klimas, *ibid.* **95**, 4155 (1990).
10. M. F. Thomsen, in *Collisionless Shocks in the Heliosphere: Reviews of Current Research*, B. T. Tsurutani and R. G. Stone, Eds. (Geophysical Monograph 35, American Geophysical Union, Washington, DC, 1985), pp. 253–270.
11. K. R. Moore, D. J. McComas, C. T. Russell, J. D. Mihalov, *J. Geophys. Res.* **94**, 3743 (1989).
12. D. J. Williams *et al.*, *Science* **253**, 1525 (1991).
13. On the day side of Venus the densities of atomic oxygen and hydrogen are approximately equal, ~100 atoms per cubic centimeter, at an altitude of 3000 km [G. M. Keating *et al.*, in *The Venus International Reference Ionosphere*, A. J. Kliore, V. I. Moroz, G. M. Keating, Eds., *COSPAR Advances in Space Research*, vol. 5, no. 11 (Pergamon, Oxford, 1985), pp. 117–171]. The hot hydrogen is not gravitationally bound and can be coarsely extrapolated to Galileo positions by assuming an inverse-square radial dependence beyond 3500 km. The atomic oxygen is mostly gravitationally bound and the densities are considerably less than those for hydrogen beyond 3500 km.
14. L. H. Brace, R. F. Theis, S. A. Curtis, L. W. Parker, *J. Geophys. Res.* **93**, 12735 (1988).
15. J. D. Mihalov and A. Barnes, *Geophys. Res. Lett.* **8**, 1277 (1981).
16. This particular coordinate system is chosen because of the convenience of computing the positions of the plasma samples in phase space. Specifically, the V_3-axis is directed parallel to **B**, and V_2 is parallel to $\mathbf{B} \times \mathbf{V}_s$, where $\mathbf{V}_s$ is the antisolar direction in a right-handed Cartesian coordinate system. The gyration speed is $V_g = |\mathbf{V}_s \times \mathbf{B}|/B$.
17. Pickup ions in the vicinity of comet Halley have been reported to be scattered in velocity space after their initial gyromotion in a ring [T. Mukai, W. Miyake, T. Terasawa, M. Kitayama, K. Hirao, *Nature* **321**, 299 (1986)].
18. E. Möbius *et al.*, *ibid.*, **318**, 426 (1985).
19. To obtain an estimate of the anticipated densities of pickup hydrogen ions, we use the atmospheric model for atomic hydrogen (*13*) and assume a one-dimensional geometry with $\mathbf{V}_s \cdot \mathbf{B} = 0$ and a radial column density of atomic hydrogen. Then the corresponding ion density is $1.5 \times 10^{11}/V_s\tau R$, where $V_s = 4.5 \times 10^7$ cm s^{-1}, R is the radial distance from Venus center to the spacecraft in units of Venus radii, and τ is the lifetime of atomic hydrogen, 1.2×10^6 s [P. D. Feldman, in *Comets*, L. L. Wilkening, Ed. (Univ. of Arizona Press, Tucson, 1982), pp. 461–479].
20. We acknowledge discussions with M. G. Kivelson, D. A. Gurnett, D. J. Williams, J. D. Mihalov, L. H. Brace, A. I. Stewart, and E. Marsch. M. G. Kivelson and D. A. Gurnett provided data from the magnetometer and plasma wave instrument, respectively. Major contributions to the implementation of the plasma instrumentation at The University of Iowa were made by J. A. Lee, M. R. English, and G. L. Pickett. The authors express their appreciation to the following personnel of the Jet Propulsion Laboratory for their contributions to our efforts: C. M. Yeates, J. R. Casani, W. G. Fawcett, H. W. Eyerly, M. S. Spehalski, W. J. O'Neil, R. F. Ebbett, T. V. Johnson, and S. J. Bolton. This research was supported in part at The University of Iowa by the Jet Propulsion Laboratory under contract 958778.

26 April 1991; accepted 9 July 1991

Images from Galileo of the Venus Cloud Deck

Michael J. S. Belton, Peter J. Gierasch, Michael D. Smith, Paul Helfenstein, Paul J. Schinder, James B. Pollack, Kathy A. Rages, Andrew P. Ingersoll, Kenneth P. Klaasen, Joseph Veverka, Clifford D. Anger, Michael H. Carr, Clark R. Chapman, Merton E. Davies, Fraser P. Fanale, Ronald Greeley, Richard Greenberg, James W. Head III, David Morrison, Gerhard Neukum, Carl B. Pilcher

Images of Venus taken at 418 (violet) and 986 [near-infrared (NIR)] nanometers show that the morphology and motions of large-scale features change with depth in the cloud deck. Poleward meridional velocities, seen in both spectral regions, are much reduced in the NIR. In the south polar region the markings in the two wavelength bands are strongly anticorrelated. The images follow the changing state of the upper cloud layer downwind of the subsolar point, and the zonal flow field shows a longitudinal periodicity that may be coupled to the formation of large-scale planetary waves. No optical lightning was detected.

The Solid State Imaging (SSI) camera on Galileo returned 77 useful images from Venus documenting the dynamical state of the cloud tops during the week after the encounter on 10 February 1990 universal time (UT). The geometry of the encounter (*1*) and the ability of the SSI camera (*2*) to image in the near-infrared (NIR) and the violet allowed an imaging sequence that probed to different depths in the cloud layers and that could follow the evolution of small-scale dynamical phenomena in the atmosphere as it flowed through the subsolar region and downwind toward the afternoon terminator. This region of the atmosphere has not undergone detailed exploration by previous missions to Venus.

Mariner 10, Pioneer Venus, Vega balloon, and recent ground-based infrared observations have provided a great deal of information about the dynamical state of the venusian clouds (*3–5*). The pressure level where the short-wavelength contrasts are formed is ~50 mbar (*6*). This is at a level some 65 to 70 km above the surface, where the temperature is about 230 K. The cloud tops are part of a deep system of haze and cloud layers, consisting of sulfuric acid droplets, that extends upward above the 45-km

M. J. S. Belton, National Optical Astronomy Observatories, Tucson, AZ 85719.
P. J. Gierasch, M. D. Smith, P. Helfenstein, P. J. Schinder, J. Veverka, Cornell University, Ithaca, NY 14853.
J. B. Pollack, K. A. Rages, D. Morrison, NASA Ames Research Center, Moffet Field, CA 94035.
A. P. Ingersoll, California Institute of Technology, Pasadena, CA 91125.
K. P. Klaasen, Jet Propulsion Laboratory, Pasadena, CA 91109.
C. D. Anger, ITRES Research Ltd., Calgary, Canada, T2E 7H7.
M. H. Carr, United States Geological Survey, Menlo Park, CA 94025.
C. R. Chapman, Planetary Science Institute, Science Applications International Corporation, Tucson, AZ 85719.
M. E. Davies, RAND Corporation, Santa Monica, CA 90406.
F. P. Fanale, Institute for Geophysics, Honolulu, HI 96822.
R. Greeley, Arizona State University, Tempe, AZ 85281.
R. Greenberg, University of Arizona, Tucson, AZ 85721.
J. W. Head III, Brown University, Providence, RI 02912.
G. Neukum, Deutsche Luft und Raumfahrt, 8031 Oberpfaffenhofen, Federal Republic of Germany.
C. B. Pilcher, NASA Headquarters, Washington, DC 20546.

level (2 bar; 370 K). There are three dominant layers (7) with additional thin, highly stratified haze layers found at great heights above the main cloud deck (*8, 9*). Features in the ultraviolet show variable zonal motions of $\sim$100 m s^{-1} over the planet's equator. This "super"-rotation is in the same direction as that of the solid planet but is about 50 times faster; it is also found to be variable on time scales of years. At high latitudes there are large-scale jets with amplitudes that also vary; these jets sometimes are absent, causing the cloud tops to follow a rigid-body rotation profile. Poleward meridional motions (up to $\sim$10 m s^{-1}) have consistently been measured, and there is evidence for a solar-locked pattern in the markings that indicates strong horizontal divergence in the flow related to the subsolar region. Finally, there is evidence for the presence of equatorial and mid-latitude planetary-scale waves that propagate in the cloud layers relative to the flow. These waves, through some mechanism not yet understood, appear to give rise to the dark markings at the largest scale.

Even with this knowledge, researchers have a poor understanding of the processes that maintain the vigorous circulation of the atmosphere (*10*). In particular, there is no observational evidence for an equatorward momentum transport, which would be an important factor in explaining the observed spin of the atmosphere. Very little is known about the dynamical transports at small spatial scales and short time scales, and the possibility that transports might be organized to provide equatorward transport of zonal momentum is of considerable interest. The capabilities of the Galileo camera permitted us to address a major part of our experiment to this question. It has been established that small-scale motions exist and can be dynamically complex. The Vega balloons in 1985 discovered vertical motions of $\sim$1 m s^{-1}, varying with time scales of a fraction of an hour in the vicinity of the middle cloud layer. In addition, recent theoretical work (*11*) has shown that trapped internal waves are possible near the cloud deck.

The Galileo camera (*2*) utilizes a virtual phase charge-coupled silicon detector with linear photometric response from 350 to 1000 nm. Broad-band spectral resolution is obtained with an eight-position filter wheel, but only the clear (633 nm), violet (418 nm), and NIR (986 nm) filters were used at Venus. The principal limitation on the experiment was the volume of data that could be accommodated on the tape recorder because the main communications antenna was not available for use. The imaging sequence (*1, 12*) was therefore limited to 81 frames.

We have used Irvine's (*13*) ground-based photometry, with phase-angle dependence, to calibrate the brightnesses in the images. We found very small residuals between observed and calculated brightnesses and obtained good removal of terminator and limb gradients with the empirical function:

$$I = B\frac{F_\odot}{\pi\mu}(\mu\mu_\odot)^k\frac{1-\exp(-\mu_\odot/a)}{1-\exp(-\mu/b)} \quad (1)$$

I is the reflected intensity and $F_\odot$ is the solar flux, both integrated over the instrument passband, $\mu_\odot$ is the cosine of the solar incidence angle (measured from vertical), and μ is the cosine of the emission angle. In the NIR, $B = 0.85$, $k = 1.14$, $a = 0.118$, and $b = 0.0019$. In the violet, $B = 0.59$, $k = 0.90$, $a = 0.0547$, and $b = 0.0039$. The fit was made at a phase angle of 47°. We used such models as a tool to remove the background run of brightness from the images so that the morphology of the smaller scale markings is easier to discern. Most of the difference between the data and model predictions is due to real contrast variations over the disk. These are about 25% in the violet and 3% in the NIR.

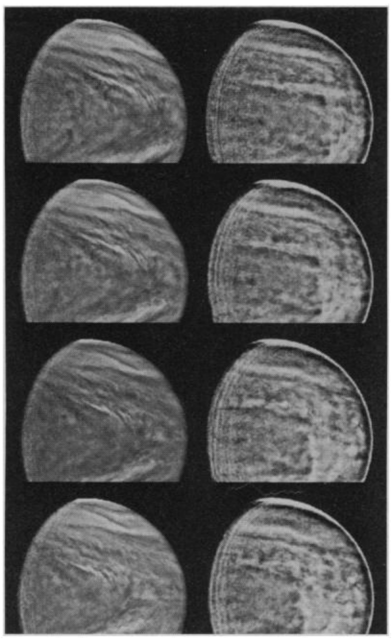

Fig. 1. Time sequence of violet and NIR image pairs. Violet frames are to the left and NIR to the right. North is at the top. The brightnesses have been divided by the mean photometric function specified in Eq. 1 to emphasize the morphology of the markings. The bright limb in the NIR images is an artifact of this process. Other artifacts are small, faint circular features, which are residual blemishes due to incomplete compensation of the shadows of small dust particles (*12*), and the faint curved lines in the terminator and subsolar regions, which are digitization contours due to the heavy stretch. Time increases from top to bottom. Within each pair the images are separated by 30 s; each row of images is separated by approximately 2.01 hours. The retrograde motion of the markings is easily seen at both wavelengths. The north-south brightness boundary stretching across the equator in the NIR frames correlates with motions in the violet frames. The frame numbers are as follows: 18494400, 18494445, 18506300, 18506345, 18518400, 18518445, 18530200, and 18530245. The resolution in the last two frames is 17 km per pixel, and the phase angle is 46°.

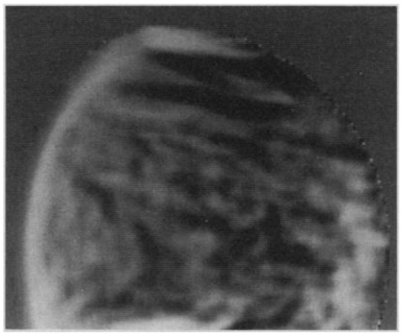

Fig. 2. Correlation image formed from the last pair displayed in Fig. 1. A correlation box about 10% of the planetary radius on a side was employed. The background shade represents no correlation. The darkest and lightest regions on the image represent correlation coefficients of about −0.7 and +0.5.

Figure 1 displays a series of NIR and violet image pairs. The violet frames show sloping striations that form a global spiral toward the pole, familiar from previous imaging experiments; on global scales the Venus cloud deck has a strikingly symmetrical and laminar-like dynamical appearance. The mottled area at low latitudes in the afternoon quadrant is also familiar and has been attributed to convection (*4*). The general pattern is consistent with formation of clouds at low latitudes with no particular alignment or elongation, followed by shearing and stretching as the clouds drift poleward (*11*). The bright collar at high latitudes is thought to be part of a polar circulation and has also been observed previously.

The patterns in the NIR image have never been observed before. There is a suggestion of a spiral pattern at mid-latitudes. The contrast in the polar regions seems to be reversed, with the bright violet collar replaced by a dark one. In addition, there is a strong discontinuity in brightness running north-south across the equator, just downwind of the subsolar region. This feature can be seen to migrate with the zonal flow through the subsolar region, apparently in step with a related feature seen in the violet (probably associated with the structures at the "root" of the horizontal Y feature often seen in images of the Venus ultraviolet markings, but only weakly evident in the Galileo images). The tilt of the mid-latitude spirals is smaller than that of the violet

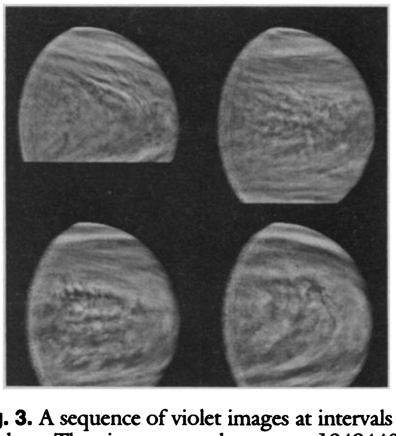

Fig. 3. A sequence of violet images at intervals of 1 day. The image numbers are 18494400, 18633900, 18773300, and 18912800. The cloud deck rotates from east to west, or from right to left, in these frames. The time sequence is from left to right and then top to bottom.

striations, although closer inspection of the violet images shows a smaller tilt for large-scale features than that for small ones. As in the violet, clouds tend to be patchy at low latitudes and linear or streaky at mid- and high latitudes. This result is consistent with the same hypothesis described above for formation of the general pattern in the violet. It suggests that the same mechanism is at work at the deeper level where the NIR contrasts are formed.

We have checked this hypothesis by studying a short movie sequence of violet feature track frames. The movie allows the eye to discern relationships that are sometimes hard to recognize on the individual pictures. We were able to identify several small-scale features migrating poleward from low latitudes and melding into the striated spiral pattern. At higher latitudes, elongated features squirt along the lanes formed by the large-scale striation pattern.

The movie sequence also shows that blotchy areas occur in patches astride the equator and that two distinct patches are separated in longitude by a few thousand kilometers. Similar patches of bright-rimmed cellular features are also seen in images taken much later in the sequence. These features may be triggered by a large-scale wave. The small blotches themselves are a few hundred kilometers in diameter and have lifetimes that can exceed 1 day (because we were able to track them for this time). They are thus much larger and slower than convective elements should be according to simple theory, which would predict dimensions on the order of a scale height (about 5 km) and time scales of less than an hour. In Earth's atmosphere, fields of convection cells are often seen with similarly large aspect ratios; however, whether they are manifestations of the same phenomena is not clear. A radiative instability (*14*) is an alternative cause of these features, as could be convective overshoot into an overlying stable region (*15*). In any of these cases small vertical shear would most likely be needed to permit unaligned features to develop. The origin of the mesoscale blotches and cellular markings remains a puzzle.

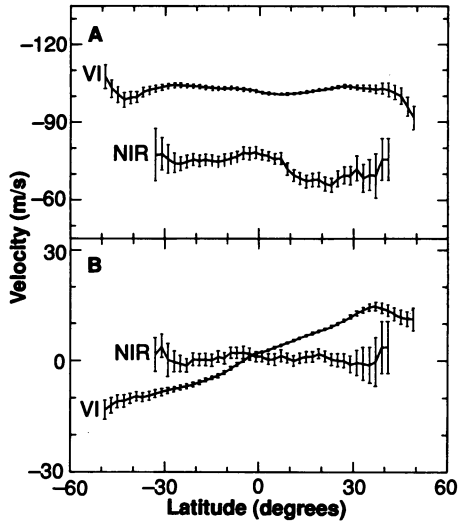

Fig. 5. Velocities of NIR and violet (VI) features as a function of latitude; (**A**) eastward, (**B**) northward. The vertical bars indicate the estimated error, based on the sample standard deviations within each 15° latitude averaging bin.

In our examination of the images we have not found any visible evidence for changes in cloud morphology on time scales less than an hour or two. Even at time separations of 2 hours we see only gradual evolution in the shape of features with lifetimes on the order of a day. Thus, we have not yet, for example, seen any evidence for small-scale internal gravity wave activity.

We have investigated whether there are cloud features in common between the NIR and violet images by forming a cross-correlation image. Using the last pair of images of Fig. 1, we evaluated the cross-correlation within a sliding box 30 pixels square (the planetary diameter is about 600 pixels) and formed the image displayed in Fig. 2. The area outside the disk is filled with a shade of gray indicating zero correlation. The darkest regions in the image represent a correlation of about −0.7. We have experimented with random patterns and believe that the anticorrelation indicated by these dark regions is meaningful. In some large areas on the images it is quite clear by inspection that an anticorrelation exists, such as near the polar collar. In low latitudes the sense of correlation is mixed, except in the region upwind of where the NIR picture shows a north-south brightness boundary and the correlation is positive.

The inverse relationship between brightnesses in the NIR and violet at high latitudes can be explained by changes in cloud density

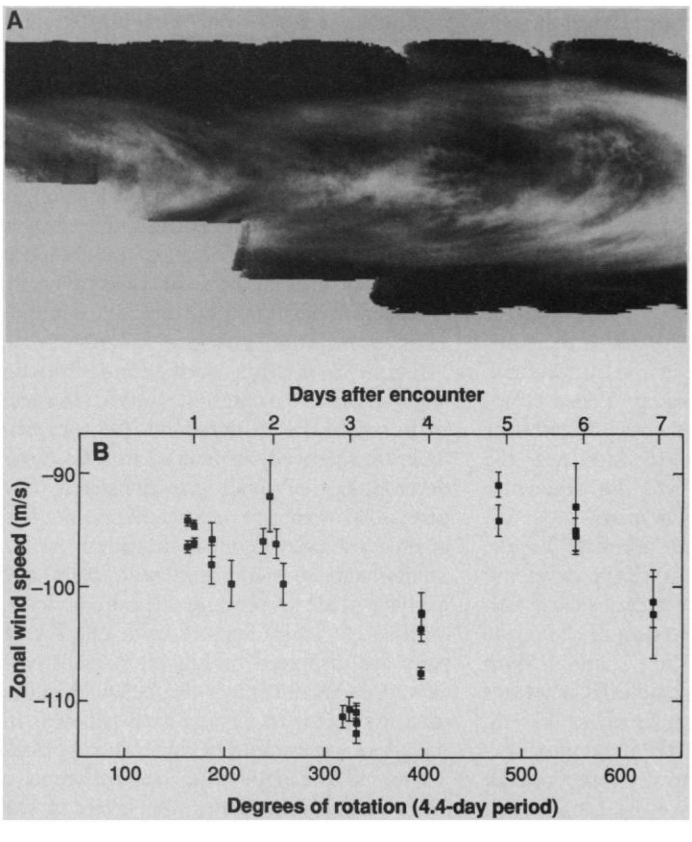

Fig. 4. (**A**) Cylindrical projection of a set of images taken over a 7-day period. A 4.4-day rotation period was adopted to define a longitude system that approximately moves with the equatorial clouds. The global dark and light pattern displays the "Y" and shows that there is a wavenumber-1 albedo variation. (**B**) The zonal wind speed, averaged over local times between 1 and 2 p.m. and latitudes 0° to 15°N, is displayed, also exhibiting a wavenumber-1 variation.

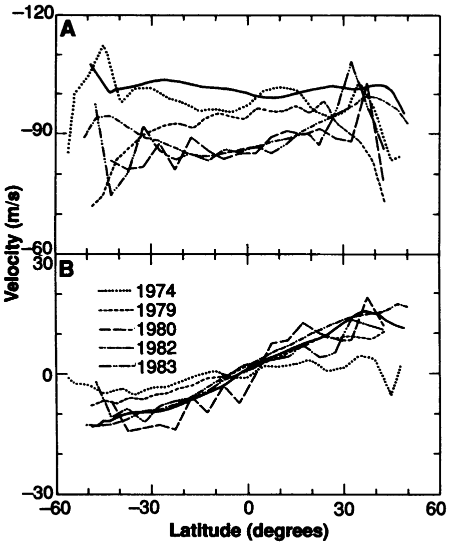

Fig. 6. Zonal mean velocities compared to earlier epochs; (**A**) eastward, (**B**) northward. The Galileo data is displayed as a solid line. Profiles from 1974 are from Limaye and Suomi (*19*). Profiles from 1979 and 1982 were measured from Pioneer Venus images by Limaye *et al.* (*20*). Profiles from 1980 and 1983 are our measurements from Pioneer Venus images.

in the altitude region between 60 and 65 km. We have used Crisp's (*16*) description of the cloud particles and optical properties to evaluate radiative fluxes in the two-stream approximation, and we examined the sensitivity of reflected fluxes to the particle number density at different heights. An increase of the cloud density between 60 and 65 km has the effect of increasing the NIR reflectivity but decreasing the violet one, because cloud particles are more absorbing in the violet. Other violet contrasts, which may or may not be correlated with the NIR brightness, can arise from cloud changes at other levels in the atmosphere.

Four violet images taken at 24-hour time intervals are displayed in Fig. 3. Because the cloud top rotation period is ~4 days, these frames show the morphology of the entire cloud deck (as well as it can be determined from monitoring one side of the planet). Frames covering the entire 7-day period of Galileo imaging are linked together in cylindrical projection in Fig. 4A. At this epoch, the large-scale dark and light patterns that sometimes form the famous "Y" feature do not seem to be strong but are evident. Patches of bright-rimmed cellular features (noted above) can also be seen in this picture. Figure 4B shows a correlation of zonal velocity measurements with this pattern, which is discussed more fully below.

The National Aeronautics and Space Administration (NASA) Jet Propulsion Laboratory (JPL) computer software program for tracking cloud patches, AMOS (*17*), has been used to measure displacements of features and to infer velocities. These velocities are true fluid velocities only if clouds act as inert tracers, which is not known to be strictly true on Venus. Belton *et al.* (*4*) have argued that because small- and moderate-scale features (up to a few hundred kilometers) seem to move together on Venus and atmospheric waves are in general dispersive, these features are unlikely to be waves. Furthermore, cloud tracking gives results that are in accord with in situ probe determinations (*18*). However, very large scale albedo features are found to move with different velocities from small tracers and have been identified with planetary-scale waves propagating in the flow (*4, 5*). In the case of the Galileo data, the results are still preliminary. We have measured 1529 tracers in violet and 126 in the NIR. The NIR features are larger than the violet ones and much more diffuse. There are a large number of violet images yet to be measured, and improved techniques are being developed to increase the accuracy with the NIR images.

Zonal mean velocities of violet features are displayed in Fig. 5. Averages were formed by binning the data in 24-hour intervals and then averaging these bins with equal weight. Thus, each sector of the rotating cloud deck is given roughly equal weight, in spite of the fact that many more tracers were located in the images of higher resolution. The average in latitude was formed with sliding bins 15° wide. The violet tracers show somewhat larger zonal winds ($u = 101 \pm 1$ m s^{-1} at the equator, where u is the eastward velocity) than those in most previous epochs (Fig. 6) (*19, 20*) and exhibit weak mid-latitude jets. The 1979 Pioneer Venus epoch stands out as showing the velocity profile most similar to solid-body rotation. Zonal mean meridional velocities are poleward, as in other epochs, and probably represent a poleward branch of a planetary Hadley circulation at cloud level.

The NIR tracers (Fig. 5) show smaller zonal velocities ($u = 78 \pm 3$ m s^{-1} at the equator), as would be expected if their origin were seated deeper in the atmosphere. Doppler tracking of Pioneer Venus atmospheric descent probes has consistently shown vertical shear of this kind near the cloud region (*18*), whereas the experience with the Venera probes is mixed (*10*). We can make a very rough estimate of the possible vertical separation of the violet and NIR markings using the average shear estimated on the basis of the sum of the probe experience, that is, ~1.5 m s^{-1} km^{-1}. With this as a guide, the violet and NIR markings could be separated by as much as 15 km, which would place the NIR markings somewhere toward the bottom of the middle cloud layer. However, we must stress that

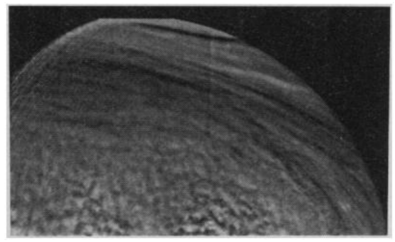

Fig. 7. High-resolution mosaic of images 18218000 and 18218045. North is to the top. The left side is afternoon and the right side is morning. The background photometric function has been removed. Note the two distinct patches of activity on the equator, separated by a low-contrast zone.

this estimate cannot be taken as much more than an educated guess. Perhaps the most interesting results on NIR motions are the extremely small meridional velocities, which indicate a very weak Hadley circulation at the level where these features originate. If we assume random measurement error, an estimate of the uncertainty can be made from the standard deviation and the number of samples. At 25° latitude this procedure yields $u = 70 \pm 3$ m s^{-1} and $v = 0.1 \pm 2$ m s^{-1}, where v is the northward velocity.

An independent estimate of the meridional drift velocity of NIR features can be made if one adopts the assumption described above that mid-latitude streaks are caused by shearing of blobs formed near the equator. The amount of shear, and therefore the tilt of streaks, is then related to the shear strength and the length of time that it takes for a blob to drift to mid-latitudes. Under these conditions, blobs stretch out to conform approximately to streamlines (*11*), as observed in the frame rotating with the equatorial velocity. The slope of streamlines is $d\lambda/d\theta = -v\cos\theta/(u - u_{eq}\cos\theta)$, where λ and θ are east longitude and latitude and u_{eq} is eastward velocity at the equator. The images show that for large-scale streaky features $d\lambda/d\theta$ is about 0.1 and that the zonal velocity is nearly independent of latitude. Solving for the meridional velocity at 30° gives $v \approx 1.2$ m s^{-1}.

Figure 7 displays a two-frame mosaic from a series of high-resolution images, again with the background photometric function removed, sequenced to follow the development of small-scale dynamical features downstream of the subsolar point. The images are rich in detail; hundreds of tie points can be located in each set of pairs, and we have made preliminary measurements of motions. Velocity vectors from one set of pairs are displayed in Fig. 8. A transition from organized, laminar-like behavior in the morning sector to disorganized behavior in the afternoon is clearly evident. Cloud deck instability forced by solar heating seems a likely cause, although at the levels in the

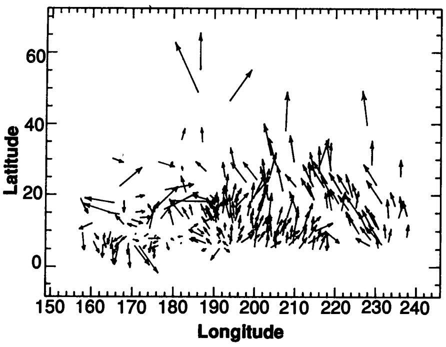

Fig. 8. Map of high-resolution velocity vectors. The mean rotation profile has been subtracted. Note the more turbulent appearance of the afternoon sector. These measurements were made from images 18229900, 18229945, 18240700, and 18240745. The arrows show the displacement that would occur in a 12-hour time period; the actual time lapse between the image pairs is 2 hours.

cloud deck associated with the violet markings, the thermal structure of the atmosphere is not susceptible to buoyant instability. There is no evidence in the Galileo images for the circumequatorial belt phenomena seen by Mariner 10 (*3–5*) or the formation of "bowlike" waves upstream of the subsolar region. There is, however, evidence for a "detached" remnant of a bowlike wave structure that can be seen propagating downstream in the image sequence in Fig. 1.

When the velocity field in solar-fixed coordinates is examined as a function of time, an interesting behavior appears. It is displayed in juxtaposition with the cylindrical projection in Fig. 4B. A periodic oscillation of the zonal velocity with an amplitude of about 10 m s^{-1} is strongly suggested, although the data do not extend over a long enough time interval to verify the periodicity. Del Genio and Rossow (*5*) discovered a similar zonal wind oscillation in Pioneer Venus data. In the Galileo observations, the oscillation exhibits a particularly large amplitude. Del Genio and Rossow attribute the oscillation to a Kelvin wave propagating slightly faster than the cloud top rotation.

If venusian lightning flashes have power characteristics and frequency of occurrence similar to that of terrestrial lightning (*21*) and spectral characteristics similar to those suggested by Borucki *et al.* (*22*), then it is only marginally possible that they could be detected by the SSI camera. Nevertheless, in view of the considerable interest in Venus lightning, ten frames were devoted to a search. No indications for the presence of lightning flashes were found in these pictures. By chance, four images included the bright star κ-Geminorum (brightness V = 3.57 magnitude; G8) at a distance of 1.3 mrad from the dark limb, and we used this object as a guide to make a rough estimate of the energy in a flash that we would have just failed to detect. We found that any Venus flashes would have had to exceed a total optical energy per flash of ~4 × 10^9 J to have been detected. This is roughly three orders of magnitude brighter than a typical terrestrial flash.

Three pairs of images of the limb of Venus were obtained through the violet and NIR filters between 1.5 and 3.6 hours after closest approach to define the vertical structure of the cloud layer above 85 km (~1 mbar; 180 K). Two pairs of images captured the limb near 48° and 57°N with resolutions of 0.5 (violet) and 0.9 km per pixel (NIR), and one pair included the limb near 2°S when the resolution had fallen to 1 and 1.8 km per pixel, respectively (these resolution estimates take into account smear during the exposures). Figure 9 illustrates the derived run of extinction coefficient with height above the surface at the three latitudes, derived with an inversion program developed to analyze limb images in the Voyager program (*23*). Allowance was made for scattering from both the direct solar beam and the light reflected from the lower lying, optically thick cloud deck with a model developed by Hapke and co-workers (*9*). The zero point for the height scale was made with the assumption that the half intensity points along the limb are at a radius of 6136 km in both filters (*12*) and that the surface is at a radius of 6051 km. The profiles should be most accurate in the altitude range from 83 to 96 km. At lower altitudes, the slant path optical depth exceeds unity, and the inversion rapidly loses accuracy; at higher altitudes, the data become too noisy. The upturn in the extinction coefficients above 96 km is an artifact of the inversion program that results from a combination of low signal-to-noise and uncertainties in the level of the zero-point brightness value. Additional uncertainties are introduced by the presence of weak ghost images induced by the front aperture cover (*12*). We have simulated the effects of these ghost images and find that they will not introduce any localized artifacts at the altitudes in the above range. The ghosts can, however, cause substantial changes in the derived extinction coefficients and aerosol scale heights. We estimate that the latter may be increased by 10 and 20% (violet and NIR, respectively) over their true values between 87 and 96 km by this effect. We have not included the influence of far-field scattered light in this preliminary analysis, but this influence is not expected to be significant.

The extinction profiles at common latitudes are effectively the same at both wavelengths and share similar shapes and magnitudes (Fig. 9). This implies that particle scattering, rather than molecular scattering,

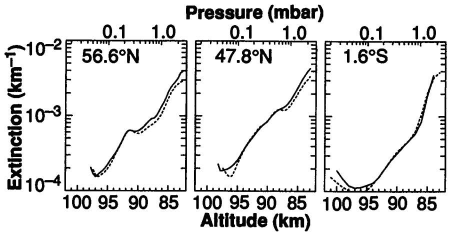

Fig. 9. Run of volume extinction coefficient with height in the cloud tops at three different latitudes. Continuous lines correspond to images taken through the violet (418 nm) filter; dashed lines correspond to the NIR (986 nm) filter. The altitude scale refers to the surface, assumed to be at a radius of 6051 km.

is chiefly responsible for the observed light at relatively high altitudes in the atmosphere and that the mean size of the scatterers is at least a few tenths of a micrometer, in accord with results from Pioneer Venus at lower altitudes (*6*). The more subdued amplitude of the prominent local maximum near 90 km at 57°N in the violet filter may indicate that Rayleigh scattering is beginning to show its presence at 418 nm (*8*).

The low latitude profiles show a smooth decline in extinction with increasing altitude with no evidence for a discrete layer. However, the extinction coefficient displays a significantly sharper decline with increasing altitude from about 84 to 87 km (scale height = 1.7 km) than from 87 to 94 km (scale height = 4.5 km, approximately the same as the local gas scale height). The higher latitude profiles differ from the above in that they show evidence for a discrete layer near 90 km and a larger scale height (~3.1 km) in the lower altitude region. Generally, the behavior of limb hazes seen by Galileo is similar to that seen in Mariner 10 images (*8, 9*). However, the local maxima on the Mariner 10 images occurred at lower altitudes (79 to 85 km) and were most marked at low latitudes, and the discrete layers had larger amplitudes than the ones seen at higher latitudes in the Galileo images obtained 15 years later.

The above comparisons imply that significant changes in the upper levels of the cloud occur on time scales of years, in accord with changes in gas abundance and particle properties derived from Pioneer Venus data at similar altitudes (*8, 24*).

REFERENCES AND NOTES

1. T. V. Johnson *et al.*, *Science* **253**, 1516 (1991).
2. K. P. Klaasen, M. C. Clary, J. R. Janesick, *Opt. Eng.* **23**, 334 (1984); M. J. S. Belton *et al.*, *Space Sci. Rev.*, in press.
3. B. C. Murray *et al.*, *Science* **183**, 1307 (1974); L. D. Travis *et al.*, *ibid.* **203**, 781 (1979); W. B. Rossow, A. D. Del Genio, S. S. Limaye, L. D. Travis, P. H. Stone, *J. Geophys. Res.* **85**, 8107 (1980); L. W. Esposito, R. G. Knollenberg, M. Ya. Marov, O. B. Toon, R. P. Turco, in *Venus*, D. M. Hunten, L.

Colin, T. M. Donahue, V. I. Moroz, Eds. (Univ. of Arizona Press, Tucson, 1983), pp. 484–564; D. Allen and J. W. Crawford, *Nature* **307**, 222 (1984); V. M. Linkin *et al.*, *Science* **231**, 1417 (1986); S. S. Limaye, *Icarus* **73**, 212 (1988); D. Crisp *et al.*, *Science* **246**, 506 (1989); W. B. Rossow, A. D. Del Genio, T. Eichler, *J. Atmos. Sci.* **47**, 2053 (1990).
4. M. J. S. Belton *et al.*, *J. Atmos. Sci.* **33**, 1383 (1976); M. J. S. Belton, G. R. Smith, G. Schubert, A. D. Del Genio, *ibid.*, p. 1394.
5. A. D. Del Genio and W. B. Rossow, *ibid.* **47**, 293 (1990).
6. K. Kawabata *et al.*, *J. Geophys. Res.* **85**, 8129 (1980).
7. R. G. Knollenberg and D. M. Hunten, *ibid.*, p. 8039.
8. B. O'Leary, *J. Atmos. Sci.* **32**, 1091 (1975).
9. D. Wallach and B. Hapke, *Icarus* **63**, 354 (1985).
10. G. Schubert, in *Venus*, D. M. Hunten, L. Colin, T. M. Donahue, V. I. Moroz, Eds. (Univ. of Arizona Press, Tucson, 1983), pp. 681–765.
11. P. J. Schinder, P. J. Gierasch, S. S. Leroy, M. D. Smith, *J. Atmos. Sci.* **47**, 2037 (1990).
12. M. J. S. Belton *et al.*, *Adv. Space Res.*, in press.
13. W. M. Irvine, *J. Atmos. Sci.* **25**, 610 (1968).
14. P. J. Gierasch, A. P. Ingersoll, R. T. Williams, *Icarus* **19**, 473 (1973); S. J. Ghan, *J. Atmos. Sci.* **46**, 2529 (1989).
15. G. Schubert, personal communication.
16. D. Crisp, *Icarus* **67**, 484 (1986); *ibid.* **77**, 391 (1989).
17. G. M. Yagi, J. J. Lorre, P. L. Jepsen, in *Proceedings of the Conference on Atmospheric Environment of Aerospace Systems and Applied Meterology* (American Meterological Society, Boston, 1978), pp. 110–117.
18. See, for example, C. C. Councelman, S. A. Gourevitch, R. W. King, G. B. Loriot, and E. S. Ginzberg [*J. Geophys. Res.* **85**, 8026 (1980)].
19. S. S. Limaye and V. E. Suomi, *J. Atmos. Sci.* **38**, 1220 (1981).
20. S. S. Limaye, C. J. Grund, S. P. Burre, *Icarus* **51**, 416 (1982); S. S. Limaye, C. Grassotti, M. J. Kuetemeyer, *ibid.* **73**, 191 (1988).
21. M. A. Williams, E. P. Krider, D. M. Hunten, *Rev. Geophys. Space Phys.* **21**, 892 (1983); Z. Levin, W. J. Borucki, O. B. Toon, *Icarus* **56**, 80 (1983).
22. W. J. Borucki *et al.*, *Geophys. Res. Lett.* **10**, 961 (1983).
23. J. B. Pollack *et al.*, *J. Geophys. Res.* **92**, 15037 (1987).
24. We gratefully acknowledge an internal review of the manuscript by G. Schubert and the assistance of H. Breneman, B. Carcich, C. Cunningham, E. DeJong, S. Howell, B. Paczkowski, T. Thompson, A. Toigo, and L. Wainio in the planning and execution of the SSI experiment and the subsequent reduction of the data.

21 June 1991; accepted 29 July 1991

Middle Infrared Thermal Maps of Venus at the Time of the Galileo Encounter

GLENN S. ORTON, JOHN CALDWELL, A. JAMES FRIEDSON, TERRY Z. MARTIN

Images of the disk of Venus, taken at wavelengths between 8 and 22 micrometers, were obtained a few days after the Galileo spacecraft's closest approach on 8 February 1990; these images show variations in the thickness of the main H_2SO_4 cloud deck and the overlying temperature structure. Several features are qualitatively similar to those of earlier observations, such as a hot region at the south pole, surrounded by a cold "collar," and brightening toward the lower latitudes, where low-contrast banding appears. The collar does have a northern counterpart that is warmer, however. Equatorial limb darkening is quantitatively similar to that of previous observations; fairly constant at wavelengths up to 20 micrometers, where limb darkening increases substantially. In contrast to what was found in previous observations, polar and equatorial limb darkening are nearly the same at most wavelengths. A longitudinal variation is observable that is consistent with a wavenumber-2 behavior and a brightness maximum near local midnight.

AS PART OF A PROGRAM TO SUPPORT Galileo Venus science analysis and compare observations of the atmosphere of Venus with previous observations of the main H_2SO_4 cloud deck and overlying temperature structure, we imaged Venus on the mornings of 10, 11, and 12 February 1990 in the middle infrared. Poor weather prevented us from observing on 8 February, the day of the spacecraft's closest approach to Venus, or the following morning. We made the observations at the National Aeronautics and Space Administration (NASA) Infrared Telescope Facility at the summit of Mauna Kea at wavelengths of 8.57, 11.52, 13.00, 18.00, 20.24, and 21.88 μm. The wavelengths were chosen for comparison with earlier ground-based images (*1, 2*) and spatially resolved spacecraft data (*3–5*); the three longest wavelengths also overlap the spectral range of the Galileo Photopolarimeter-Radiometer (PPR) radiometric channels A, B, and C. The 60 pixel by 60 pixel images were produced by raster scanning in a regular grid pattern with 1–arc sec spacing in both directions; the entrance aperture was just under 2 arc sec in diameter. The disk of Venus, 23 to 25 days past inferior conjunction, subtended 49 arc sec, and the evening terminator was located about 42° east (Fig. 1) of the central meridian. We used the results of well-calibrated spacecraft experiments (*4, 5*) to normalize our absolute intensities.

G. S. Orton, A. J. Friedson, T. Z. Martin, Jet Propulsion Laboratory, California Institute of Technology, 4800 Oak Grove Drive, MS 169-237, Pasadena, CA 91109.
J. Caldwell, Physics Department, York University, 4700 Keele Street, North York, Ontario, Canada M3J 1P3.

The images from wavelengths of 8.57 and 11.52 μm (Fig. 1) show the greatest intensity contrast across the disk, a result of the strong dependence of their brightness on temperature. The east-west orientation of the scan rows is evident as narrow streaks, particularly near the limb of Venus, arising from short-term seeing and transparency variations. Evident in most of these images is a hot feature at the south pole. Hot features have been observed at the poles since the earliest thermal maps (*6*). This feature is consistent with Pioneer Venus Orbiter Infrared Radiometer (OIR) observations (*7*) of a bright, elongated feature at the north pole, rotating retrograde with a period of some 3 days. A much cooler "collar" surrounds the hot pole. Closer to the equator, the planet is brighter and contains lower contrast bands. None of these features is axisymmetric or stationary in earth- or solar-fixed coordinates.

The cold circumpolar collar and the brighter bands can also be seen in mosaics created from the images at each wavelength (Fig. 2). The direction of scans is evident as the nearly horizontal narrow bands sloping slightly upward toward higher longitudes. The best match of features contained in separate images implies an offset of roughly 90° in longitude per earth day, consistent with the 4-day retrograde period associated with ultraviolet features (*8*). The hot polar feature is confined to latitudes poleward of about 70°, and the collar is confined to latitudes between 50° and 70°, also consistent with the Pioneer Venus OIR results (*4, 7*). Except at 8.57 μm, the mosaics also show a cool region poleward of 45°N. The presence of a northern counterpart of the south pole collar is consistent with Galileo PPR maps and Near Infrared Mapping Spectrometer (NIMS) images of Venus from 5-μm thermal emission from the same cloud deck (*9*), but this collar is warmer than its southern counterpart. Images of the thermal emission of the night side of Venus at shorter wavelengths (*9, 10*) show a dark area near the pole that could correspond to the collar. Figure 2 shows a relatively bright streak between 30° and 50°S and a fainter streak between 20° and 40°S. There is no morphology in the Venus night side near-infrared data (*9, 10*) that immediately corresponds with these features. If the streaks are caused by a variation of cloud optical thickness, the cloud layer in question may be only one of several different components of a cloud system discernible at the shorter wavelengths.

The general morphology of brightness temperature features on Venus appears to be similar for all wavelengths greater than 8.57 μm, even at 13.00 and 18.00 μm, where the